

Abstract

It is widely believed that multidecadal to centennial cooling and drought occurred from 4500 BP to 3900 BP, known as the 4.2 ka BP event that triggered the collapse of several cultures. However, whether this event was a global event or a regional event and what caused this event remain unclear. In this study, we investigated the spatiotemporal characteristics, the possible causes and the related physical processes of the event using a set of long-term climate simulations, including one all-forcing experiment and four single-forcing experiments. The results derived from the all-forcing experiment show that this event occurs over most parts of the Northern Hemisphere (NH), indicating that this event could have been a hemispheric event. The cooler NH and warmer Southern Hemisphere (SH) illustrate that this event could be related to the slowdown of the Atlantic Meridional Overturning Circulation (AMOC). The comparison between the all-forcing experiment and the single-forcing experiments indicates that this event might be caused by internal variability, while external forcings such as orbital and greenhouse gases might have modulation effects. A positive North Atlantic Oscillation (NAO)-like pattern in the atmosphere (low troposphere) triggered a negative Atlantic Multidecadal Oscillation (AMO)-like pattern in the ocean, which then triggered a Circumglobal Teleconnection (CGT)-like wave train pattern in the atmosphere (high troposphere). The positive NAO-like pattern and the CGT-like pattern are the direct physical processes that lead to the NH cooling and megadrought. The AMO-like pattern plays a “bridge” role in maintaining this barotropic structure in the atmosphere at a multidecadal-centennial time scale. Our work provides a global image and dynamic background to help better understand the 4.2 ka BP event.

46 **1 Introduction**

47 Understanding the characteristics and mechanisms of climate changes during the
48 Holocene can help predicting future changes. The multidecadal-to-centennial abrupt
49 climate change, or the rapid climatic change during ca. 4.5-3.9 ka BP (before 1950 CE),
50 the so called “4.2 ka BP event”, was one of the major climate events during the
51 Holocene (Wang, 2009; Staubwasser and Weiss, 2006; Mayewski et al., 2004; Wang,
52 2010). This event is considered to be closely linked to the cultural evolutions of
53 different regions of Eurasia such as the collapse of the Akkadian empire, the termination
54 of the urban Harappan civilization in the Indus valley and the collapse of Neolithic
55 Cultures around the Central Plain of China (Weiss et al., 1993; Weiss and Bradley, 2001;
56 Wu and Liu, 2001; Staubwasser et al., 2003; Wu and Liu, 2004; An et al., 2005;
57 Staubwasser and Weiss, 2006; Liu et al., 2013; Weiss, 2015, 2016). Moreover, this event
58 is also thought to be the transition of the Middle to Late Holocene (Walker et al., 2012;
59 Finkenbinder et al., 2016). However, the characteristics, causes and corresponding
60 mechanisms behind this event remain unclear.

61 The 4.2 ka BP event is mostly characterized by rapid events at various latitudes
62 (Jansen et al., 2007), e.g., cooling in Europe (Lauritzen, 2003), centennial
63 megadroughts in North America (Booth et al., 2005), decreased precipitation in both
64 southern and northern China (Tan et al., 2008), and the weakened summer monsoon in
65 India (Nakamura et al., 2016); however, the manifestation of this event is far from
66 convincing and needs more evidence and simulation investigations (Roland et al., 2014).
67 Many reconstructions have shown that the 4.2 ka BP event is dominated by
68 megadroughts at centennial-scale over mid-low latitudes (Tan et al., 2008; Yang et al.,
69 2015; Weiss, 2016). However, Roland et al. (2014) found no compelling evidence, at
70 least in peatland records, to support that there was a 4.2 ka BP event in Great Britain
71 and Ireland. Moreover, according to the hydrologic cycle (i.e. the hydroclimate changes
72 are often regionally specific), it cannot be ruled out that there were no flooding events
73 somewhere else during this period. For example, Huang et al. (2011) and Tan et al.
74 (2018) found that successive floods occurred over the middle reaches of the Yellow
75 River in China in association with the abrupt climatic event of 4.2 ka BP.

76 Understanding the causes and mechanisms of the 4.2 ka BP event can provide
77 explanations for the reconstructed discrepancies over different regions. For the causes
78 of the event, some reconstruction and modeling studies have suggested that the solar
79 irradiance could have played an important role in the early Holocene climate changes
80 (Wang et al., 2005; Rupper et al., 2009; Owen and Dortch, 2014); however, no strong
81 evidence has shown that the solar irradiance affected glacier fluctuations (cooling
82 events) in the late Holocene since there is yet no good mechanistic explanations of how
83 small changes in solar irradiance could significantly affect large scale climate changes
84 (Solomina et al., 2015). Tan et al. (2008) thought that the 4.2 ka BP event could have
85 been induced by the southward shift of the Intertropical Convergence Zone (ITCZ) and
86 oceanic sea surface temperature (SST) changes, as well as the vegetation feedback
87 caused by the solar activity. Liu et al. (2013) and Deininger et al. (2017) argued that the
88 atmospheric circulation, such as the North Atlantic Oscillation (NAO)-like pattern but
89 on a centennial time scale, could have played a more important role than the ocean
90 circulation in this event, although the mechanisms that forced the circulation change
91 remained unclear. A new reconstruction study has also shown that the dry phases over
92 the western Mediterranean in the period of 4.5 ka BP-2.8 ka BP generally agreed with
93 positive NAO conditions (Ramos-Román et al., 2018). However, studies come to
94 different conclusions on the likely phase of the NAO-like patten during the late
95 Holocene (Finkenbinder et al., 2016). Some studies show positive NAO-type patterns
96 during the late Holocene (Tremblay et al., 1997; Sachs, 2007; Ramos-Román et al.,
97 2018), whereas others show negative NAO-like patterns (Rimbu et al., 2004). Since the
98 mechanisms could be a complex set of air-sea interactions (Roland et al., 2014), it is
99 hard for reconstruction to provide a general record due to its limitations such as
100 interpretation and spatially incompleteness. The mechanisms behind the 4.2 ka BP
101 event need to be clarified.

102 Therefore, to improve understanding of the 4.2 ka BP event, new high-resolution
103 reconstruction studies that focus on the 4.2 ka BP event are required. On the other hand,
104 physical-based modeling research can provide general concepts of the characteristics
105 of the event along with the causes and the mechanisms. Climate simulations have been

106 conducted to investigate another abrupt cooling event in the early Holocene, the so-
107 called 8.2 ka BP event. The simulations were used to test the hypothesis raised by the
108 reconstruction studies that the 8.2 ka BP event was most likely caused by freshwater
109 forcing and was associated with weakening of the Atlantic Meridional Overturning
110 Circulation (AMOC) (Morrill et al., 2013; Wagner et al., 2013; Morrill et al., 2014;
111 Matero et al., 2017; Ljung et al., 2008; Alley and Agustsdottir, 2005). For example, the
112 simulations argued that the meltwater from the collapse of the ice dome over Hudson
113 Bay was an essential forcing of the 8.2 ka BP event (Wagner et al., 2013; Matero et al.,
114 2017). However, little modeling work has been applied to the 4.2 ka BP event.

115 Recently, Ning et al. (2019) briefly compared the spatial patterns of climate change
116 in the 9th and 5th millennia BP using a set of transient modeling results on a long-term
117 perspective. In the present study, we will use the same set of simulation results to
118 provide an in-depth characteristics of the 4.2 ka BP event and will focus on the possible
119 causes and mechanisms behind this event. The model and experiments are introduced
120 in Sect. 2. The results are shown in Sect. 3. The possible causes and mechanisms are
121 discussed in Sect. 4, and conclusions are drawn in Sect. 5.

122

123 **2 Model and experiments**

124 A set of transient simulations (TraCE-21ka, Simulation of Transient Climate
125 Evolution over the past 21,000 years, He, 2011) conducted with the Community
126 Climate System model version 3 (CCSM3) was used to investigate the spatial and
127 temporal characteristics of the 4.2 ka BP event and to determine the possible causes and
128 mechanisms behind this event. The experiments are listed in Table 1, including one
129 transient experiment with all-forcings (TraCE-ALL), one single-forcing experiment
130 forced only by transient orbital variation (TraCE-ORB), one single-forcing experiment
131 forced only by transient melt-water flux (TraCE-MWF), one single-forcing experiment
132 forced only by quasi-transient ice-sheet (TraCE-ICE), and one single-forcing
133 experiment forced only by transient greenhouse gases concentrations changes (TraCE-
134 GHG). The simulations were conducted from 22000 BP to 1990 CE for the TraCE-ALL,
135 the TraCE-ORB and the TraCE-GHG experiments, and from 19000 BP to 1990 CE for

136 the TraCE-MWF and the TraCE-ICE experiments.

137 The transient June insolation changes at 60°N and 60°S that resulted from the
138 orbital variation and the transient CO₂ change used in the simulations are shown in Fig.
139 1. The continental ice-sheet and topography changes are based on the ICE-5G (VM2)
140 reconstruction (He et al., 2013; Peltier, 2004). For the geography changes, the Barents
141 Sea opens at 13.1 ka BP, the Bering Strait opens at 12.9 ka BP, Hudson Bay opens at
142 7.6 ka BP, and the Indonesian Throughflow opens at 6.2 ka BP. The freshwater injected
143 into Northern Hemisphere (NH) and Southern Hemisphere (SH) oceans are based on
144 specific time slices (e.g., 19 ka BP into North Atlantic, 17 ka BP into North Atlantic,
145 11.5 ka BP into Arctic, St. Lawrence River, Hudson Strait, Barents Sea, North Sea, Ross
146 Sea and Weddell Sea). Note that no freshwater was delivered to the ocean after 5000
147 BP in the TraCE-ALL and TraCE-MWF experiments. The detailed information about
148 the experiments design can be referred to He (2011) and He et al. (2013).

149 The TraCE-21ka simulation was evaluated with reconstructions and was found
150 that it could reproduce major deglacial temperature evolutions (Clark et al., 2012;
151 Shakun et al., 2012). It has been used to depict the causes and mechanisms of Holocene
152 climate changes, such as the Bølling-Allerød warming (Liu et al., 2009), cooling into
153 the Younger Dryas and recovery to warm conditions (Liu et al., 2012) and the ENSO
154 evolution over the past 21 ka (Liu et al., 2014a). In the present work, we adopted the
155 period of 5000 BP-3000 BP to focus on the 4.2 ka BP event.

156

157 **3 Results**

158 3.1 Identification of 4.2 ka BP event in the model simulation

159 The 101-year running mean annual NH surface temperature and precipitation
160 during 5 ka BP-3 ka BP shows double peak centennial cooling and drought from 4.4 ka
161 BP to 4.0 ka BP (Fig. 2, dashed black line). However, the variabilities are smaller over
162 the SH than those over the NH. There is no significant cooling and drought event during
163 that period (Fig. S1, dashed black line) over the SH. The SH precipitation even shows
164 a double-peak wet condition during the period of 4.4 ka BP-4.0 ka BP.

165 The double peak centennial cooling and drought are still obvious when the 31-year

166 running mean is applied to the time series (not shown), which indicates that the
167 simulated climate events potentially comparable to the 4.2 ka event. Moreover, the
168 centennial warming periods right before and after the cooling event indicate that this
169 event might be included in a quasi-millennium variation. Therefore, the 4.2 ka BP event
170 could be a multiscale event, i.e. from multi-decadal to millennium.

171 The seasonal mean NH surface temperature changes show that the annual mean
172 variability is dominated by the boreal winter (December-January-February, DJF)
173 surface temperature change (Fig. S2). The correlation coefficient between the annual
174 mean NH surface temperature (NHT) and the DJF mean NHT is 0.96 (after the 101-
175 year running mean), which is significant above the 99% confidence level, much higher
176 than the correlation coefficient between the annual mean and the boreal summer (June-
177 July-August, JJA) mean of only 0.30 (after the 101-year running mean), which is not
178 significant. However, this is different for the precipitation change, for which both the
179 JJA mean and the DJF mean contribute to the annual mean precipitation change (not
180 shown).

181 To identify the characteristics of the 4.2 ka BP event, two centennial cool periods
182 and two centennial warm periods that exceeded ± 0.5 standard deviations are selected.
183 The two centennial cool periods span from 4320 BP to 4220 BP and from 4150 BP to
184 4050 BP, and the two centennial warm periods span from 4710 BP to 4610 BP and from
185 3980 BP to 3880 BP.

186

187 3.2 Spatial characteristics of surface temperature and precipitation

188 To help draw a coherent global view of the 4.2 ka BP event, the spatial
189 characteristics of temperature and precipitation changes during the 4.2 ka BP event are
190 shown in Fig. 3.

191 Figure 3a gives the spatial distribution of the annual mean surface temperature
192 difference between the cold periods and the warm periods. The cooling significantly
193 occurred over most regions of the NH, especially over the middle to high latitudes of
194 the NH and most land regions of the SH. Most parts of India, northern Mexico and the
195 middle latitudes of the SH ocean experienced warm conditions. Such asymmetric

196 change between the hemispheres (cool NH and warm SH) favors the southward shift of
197 the ITCZ. The spatial distribution of the surface temperature change is still dominated
198 by the boreal winter pattern (not shown). The large cooling over the NH and small
199 warming over the SH could be related to the orbital change (Fig. S3), which induces
200 insolation increasing over the SH but decreasing over the NH.

201 The spatial distribution of annual mean precipitation differences between the cold
202 periods and the warm periods is shown in Fig. 3b. During the cold periods, significant
203 drought is mainly located over many land regions of the NH, especially over Europe,
204 western Asia, and interior North America and Central America. The significant dry
205 conditions over the Dead Sea, the Gulf of Omen, interior North America and western
206 North Africa and the wet condition over South America are consistent with the
207 reconstructions (Yechieli et al., 1993; Cullen et al., 2000; Forman et al., 1995; Marchant
208 and Hooghiemstra, 2004). For the SH, the land precipitation increased, which indicates a
209 southward shift of the ITCZ, as suggested by the aforementioned asymmetric
210 temperature change and by the previous studies based on both reconstructions
211 (Fleitmann et al., 2007; Cai et al., 2012) and simulations (Broccoli et al., 2006). Over
212 East China, the precipitation anomalies show a wet south-dry north pattern, which
213 indicates a weakened East Asian monsoon revealed by the reconstruction record (Tan
214 et al., 2018). However, the simulated anomaly pattern is not very significant over East
215 China. This might be related to the model resolution, the model performance, or the
216 actual climate change. Therefore, simulations with higher resolution, inter-model and
217 model-data comparisons are required to draw a clearer view about the climate change
218 over East China.

219 The sea surface temperature (SST) shows that the largest change occurs over the
220 northern Atlantic Ocean and then the northern Pacific Ocean (Fig. 4). The warmer south
221 and cooler north over the Atlantic Ocean indicates an Atlantic Multi-Decadal
222 Oscillation (AMO)-like pattern with its cold phase. The cold phase of the AMO has
223 been confirmed to induce summer rainfall decreases over India and Sahel in both
224 simulations and proxy data (Zhang and Delworth, 2006; Shanahan et al., 2009).

225 The simulated characteristics of the temperature change, the precipitation change,

226 and the SST change are similar to those responses to the weakened AMOC state
227 (Vellinga and Wood, 2002; Zhang and Delworth, 2005; Delworth and Zeng, 2012;
228 Brown and Galbraith, 2016) (Fig. S4).

229

230 3.3 Circulations associate with the 4.2 ka BP event

231 The sea level pressure (SLP) differences between the cooler periods and the
232 warmer periods show that the largest change occurs over the mid-high latitudes of the
233 NH and SH (Fig. 5a). The negative SLP anomalies over the high North Atlantic and
234 positive SLP anomalies over the middle North Atlantic during the cool periods resemble
235 a positive North Atlantic Oscillation (NAO)-like pattern but on a centennial-millennial
236 time scale. The positive NAO-like pattern is accompanied by cyclonic circulation over
237 Iceland and anticyclonic circulation over the Azores Islands and thus strengthened
238 westerlies over the downstream regions (Fig. 5a). The subtropical highs and the relative
239 anticyclones in both the SH and NH are strengthened during the cold periods from low
240 troposphere (850 hPa) to high troposphere (200 hPa), which illustrates a barotropic
241 structure (Fig. 5). Note that the strengthened subtropical highs over the NH are most
242 significant at low level (sea level and 850 hPa), while the subtropical highs over the SH
243 are most significant at high level (200 hPa). The centers with positive geopotential
244 height anomalies during the 4.2 ka BP event over Western Europe, Central Asia, East
245 Asia, the east north Pacific and Eastern North America, as well as the anti-cyclonic
246 circulation anomalies at 200 hPa (Fig. 5d), resemble a Circumglobal Teleconnection
247 (CGT)-like wave pattern (Ding and Wang, 2005; Lin et al., 2016) but on a centennial-
248 millennial time scale.

249 The strengthened subtropical highs with mid-latitudes anticyclones from lower to
250 upper levels are the direct physical processes that cause the precipitation decreases and
251 thus the following megadrought over mid-latitudes of NH regions, particularly over
252 Eurasia. The cooler land-warmer ocean over East Asia and the West Pacific (Fig. 3a)
253 indicate weakened land-ocean thermal contrast associated with significantly higher SLP
254 over land and lower SLP over the adjacent ocean (insignificant) (Fig. 5a). The
255 weakened land-ocean contrast can lead to a weaker East Asian monsoon, accompanied

256 by precipitation increases over the southern China pattern and precipitation decreases
257 over the northern China pattern (Fig. 3b). Such conclusion is very rough, since the
258 simulated anomaly patterns are not very significant. More investigations with higher
259 resolutions of modeling and reconstruction works are required to get satisfactory results.

260

261 **4 Discussions**

262 The simulations show that the cool and dry conditions of the 4.2 ka BP event is
263 more like a hemispheric phenomenon, mainly located over the NH, rather than a global
264 phenomenon. The land over the SH experiences cool but wet conditions, and the mid-
265 latitude SH ocean is warmer. The potential causes and mechanisms of this event will be
266 discussed in this section.

267 4.1 The possible causes of the 4.2 ka BP event

268 Some records suggested that solar irradiance was one of the essential mechanisms
269 that drove the Holocene climate variation at centennial to millennial time scales (Bond
270 et al., 2001), whereas others suggested that the linkage between solar irradiance and
271 multicentury scale cooling events during the Holocene was weak, particularly in the
272 mid- to late-Holocene (Turney et al., 2005; Wanner et al., 2008). Changes in solar
273 irradiance are not included in the experiments used in the present work. Nonetheless,
274 we still obtain multicentury cooling events (such as the 4.2 ka BP event) in the TraCE-
275 ALL experiment, but with smaller magnitude. This side-fact indicates that the solar
276 irradiance might not be the driving factor for the Holocene cooling events.

277 If the results derived from the TraCE-ALL experiment are consistent with those
278 derived from a particular single-forcing sensitivity experiment, we assume the variation
279 to be forced by that forcing. Otherwise, if the results derived from the TraCE-ALL
280 experiment differ from those from the single-forcing sensitivity experiments, we
281 assume the variation to be forced by the internal variability. In this section, we use the
282 series after applications of 101-year running means as an example and compare the
283 results derived from the all-forcing experiment to those derived from the single-forcing
284 experiment to determine the possible forcings that triggered the 4.2 ka BP event.

285 The correlation coefficients between the annual mean NHT derived from the

286 TraCE-ALL run and the NHT derived from each single-forcing run are listed in Table
287 2. A two-sided Students t-test is used for the statistical significant test, assuming 20
288 degrees of freedom, which is estimated simply from a 2000-year time series subjected
289 to a 100-year running mean (Delworth and Zeng, 2012). There is no significant clue
290 that the annual mean NHT variation is forced by the orbital variation or the other
291 forcings due to the non-significant correlations. During the period of 5000 BP - 3000
292 BP, the variation of simulated JJA mean NHT is likely forced by the solar radiation due
293 to the orbital variation (Table 2; the correlation coefficient between the two series is
294 0.79 at $p < 0.05$), whereas the greenhouse gas change has a comparable negative impact
295 on the JJA mean NHT (the correlation coefficient is -0.73 at $p < 0.05$). The melt-water
296 flux also has a moderate contribution to the JJA mean NHT change (the correlation
297 coefficient is 0.48 at $p < 0.05$). For the DJF mean NHT, only melt-water flux has a
298 notable negative effect (the correlation coefficient is -0.43 at $p < 0.05$). However, there
299 is no meltwater forcing during this period, so the NHT change can be taken as internal
300 variability. Therefore, the significant correlation coefficient between the all forcing run
301 result and the meltwater forcing run result might be a coincidence, due to the
302 autocorrelation of internal variability. This is another side-fact indicating the cold
303 events during the late Holocene might be related to the internal variability. Note that if
304 the effective degree of freedom is used, none of the abovementioned correlation
305 coefficients are significant. The effective degree of freedom is calculated by the
306 following equation:

$$307 \quad N_{dof} = N \times \frac{1 - r_1 \times r_2}{1 + r_1 \times r_2}$$

308 where N_{dof} is the effective degree of freedom regarding to the two correlation samples,
309 N is the total sample size, r_1 and r_2 are autocorrelation lag-1 values for sample 1 and
310 sample 2, respectively (Bretherton et al., 1999).

311 On the other hand, the annual mean NHT difference between the TraCE-ALL run
312 and the sum of the 4 single-forcing sensitivity experiments shows variation similar to
313 the NHT derived from the TraCE-ALL run from 5000 BP to 3000 BP (Fig. S5). The
314 correlation coefficient between these two time-series is 0.66, which is significant above

315 the 95% confidence level (assuming 20 degrees of freedom). We assume the difference
316 between the TraCE-ALL run and the sum of the 4 single forcing runs to be the internal
317 variation, taking that the climate responses to the external forcings are linear at global
318 and hemispheric scales. Therefore, the internal variation might play a dominant role in
319 the climatic variation during the period of 5000 BP-3000 BP. However, the linearity of
320 the climate responding to the external forcings need further clarification, since there
321 would be interactions between each forcing and between forcings and internal
322 variability.

323 Moreover, there is no double-peak cooling event during the period of 4400 BP-
324 4000 BP in any single forcing run (Fig. 1, colored lines), which indicates that the 4.2
325 ka BP event might not be triggered by those external forcings, including the orbital, the
326 melt-water flux, the ice-sheets and the greenhouse gases in isolation. Volcanic eruptions
327 have been identified as one of the important drivers of climate variation, whereas there
328 were few eruptions during 4400 BP-4000 BP (Sigl et al., 2018). Therefore, we conclude
329 that the variability relating to the 4.2 ka BP event might be driven by the internal
330 variability. Klus et al. (2017) also suggested that the internal climate variability could
331 trigger abrupt cold events in the North Atlantic without external forcings (e.g., solar
332 irradiance or volcanic).

333 However, why such large variation due to the internal variability occurs at
334 approximately 4.2 ka BP remains unknown. There is little ice-sheet change and no melt
335 water discharge after 5.0 ka BP in the TraCE-ICE run and TraCE-MWF run, and the
336 variations of climate derived from these two runs can thus be considered as internal
337 variabilities. The multicentennial cooling events can also be found in the standardized
338 NHT during the last 5000 years of the two experiments (Fig. S6), and there are drought
339 events in the standardized NH precipitation time series (not shown). However, the
340 timing of those cooling and drought events occurs stochastically. This indicates a
341 general concept of the random variation of the internal mode of the climate system.
342 There is a reduction of NH temperature and precipitation at around 4600 BP in the
343 TraCE-ORB (Fig. 2, orange lines), which might be related to the timing of the event as
344 speculated by Ning et al. (2019).

345 Ning et al. (2019) compared the 5th millennium BP cooling with the 9th millennium
346 cooling and concluded that the 9th millennium BP cooling was resulted from the
347 freshwater forcing while the orbital forcing is the most likely explanation of cooling in
348 the North Atlantic starting from the early 5th Millennium BP through most of the later
349 Holocene, but with fluctuations. In the present work, we attribute this fluctuation to the
350 internal variability, which is superposed on the orbital induced long-term trend. This
351 work and Ning et al.'s work (2019) focus on different aspects and different time scales,
352 and are complementary to better understand the 4.2 ka BP event.

353

354 4.2 The mechanisms of the centennial-millennial cooling and drought

355 As has mentioned in Sec. 3.3, the low level NAO-like pattern and upper level
356 CGT-like pattern are the direct mechanisms that cause cooling and megadroughts over
357 most part of the NH. Previous studies also proposed that the temperature and
358 precipitation changes over Eurasia and Africa were directly linked to the NAO (Cullen
359 et al., 2002; Kushnir and Stein, 2010). The first leading mode of the Empirical
360 Orthogonal Function (EOF) of the annual mean SLP during 5 ka BP-3 ka BP shows a
361 double-peak positive NAO-like pattern but on a centennial scale during the period of
362 4400 BP-4000 BP (Fig. 6). The first leading EOF of geopotential height at 200 hPa after
363 application of a 31-year running mean shows a CGT-like pattern and similar double-
364 peak variation during the period of 4400 BP-4000 BP, which is more obvious after
365 applying the 101-year running mean (Fig. 7). This means that the double-peak cooling
366 and drought of the 4.2 ka BP event could be strongly related to the double peak positive
367 NAO-like pattern (at low level) and CGT-like pattern (at high level) at a centennial time
368 scale.

369 Li et al. (2013) suggested that the NAO is a predictor of NHT multidecadal
370 variability during the 20th century. In this study, significant correlation is also found
371 between the annual mean NAO index and the annual mean NHT during the period of
372 4400 BP-4000 BP, with the NAO leading by approximately 40 years (Fig. 8). The NAO
373 index is defined by the first leading mode of the EOF of the SLP. The regressed annual
374 mean surface temperature against the NAO index 40 years earlier during 4400 BP and

375 4000 BP shows cooler NH high latitudes and a warmer SH (Fig. S7), especially the
376 cooling over the northern North Atlantic Ocean, Europe, East Asia and North America.

377 The geopotential height at 200 hPa regressed against the SST over the two North
378 Atlantic outstanding regions (Fig. 4) shows a CGT-like pattern after application of a
379 31-year running mean (Fig. 9), which is similar to the conclusion from Lin et al. (2016)
380 that the CGT could be excited by the AMO-related SST anomaly. The regressed 200
381 hPa geopotential height shows a similar pattern after application of a 101-year running
382 mean (not shown). The anticyclones associated with CGT-like pattern over the West
383 Europe, Central Asia and North America can suppress the precipitation and thus lead to
384 megadrought over these regions.

385 Considering the NAO-like pattern, the CGT-like pattern and the AMO-like pattern
386 together, we suggest that the AMO could be playing a “bridge” role to keep the
387 barotropic structure at the centennial scale, which is similar to the synthesis proposed
388 by Li et al. (2013) that the AMO is a “bridge” that links the NAO and NHT at a
389 multidecadal timescale. Delworth and Zeng (2016) suggested that the NAO variation
390 had significant impact on the AMOC and the subsequent influence on the atmosphere
391 and large-scale climate at multidecadal-centennial time scales. Other studies also
392 focused on the role of SST anomalies over the North Pacific and North Atlantic oceans
393 when investigating the possible mechanisms of the 4.2 ka BP event (Kim et al., 2004;
394 Marchant and Hooghiemstra, 2004; Booth et al., 2005).

395 We notice the centennial-millennial variation of the AMOC after the mid-
396 Holocene in the all forcing run (Fig. S4a). There also exists a double peak variation
397 during the period of 4.4-4.0 ka BP, accompanied by the similar spatial patterns of
398 temperature and precipitation anomalies as the simulated 4.2 ka BP event (Fig. S4b, c).
399 However, whether this AMOC variation is related to the external forcing, such as the
400 orbital forcing, or just the internal variability remains unknown, and needs further
401 investigations.

402

403 **5 Conclusion**

404 The characteristics of the 4.2 ka BP event along with the potential drivers and the

405 mechanisms are investigated using a set of transient climate simulations. The simulated
406 event is characterized by hemispheric cooling and megadrought over the NH, whereas
407 the SH experiences warming (over mid-latitude ocean) and wet conditions during this
408 event. The annual mean temperature change is dominated by the boreal winter change.
409 The cool and dry NH and warm and wet SH pattern indicates a southward shift of the
410 ITCZ, as suggested by the reconstructions. These characteristics could also be related
411 to a weakening of the AMOC, which needs further investigation.

412 By comparison between the all-forcing experiment and the single-forcing
413 sensitivity experiments, the 4.2 ka BP event can largely be attributed to the internal
414 variability, although the orbital forcing and the greenhouse gases could impact the
415 boreal summer NHT variation. The origin could be in polar regions and the North
416 Atlantic and may influence the NH climate through teleconnections such as the NAO-
417 like pattern and the CGT-like pattern. The positive NAO-like pattern in the atmosphere
418 triggers cooling over the NH and the negative AMO-like pattern in the ocean, which
419 may last for decades or even centuries. The negative AMO-like pattern triggers CGT-
420 like wave patterns at a multidecadal-centennial time scale accompanied by anticyclones
421 over West Europe, Central Asia and North America, which induce megadrought over
422 those regions. The simplified diagram of the mechanism is shown in Fig. 10.

423 Our findings provide a global pattern and mechanical background of the 4.2 ka BP
424 event that can help better understanding this event. We attribute the internal variabilities
425 to be an essential forcing of the 4.2 ka BP event. However, whether or not the external
426 forcings have modulation effects need to be clarified. For example, is the timing of the
427 event stochastic due to the internal variability or modulated by the external forcings
428 such as the orbital changes? Why the SST forcing in the North Atlantic can be
429 maintained at a multidecadal-centennial time scale requires more study. Current results
430 are mainly based on annual mean precipitation and temperature, whereas the impacts
431 of external forcings may have seasonal dependence; further investigations are required
432 to evaluate these impacts.

433 The model responses to the external forcings are small, especially in the Holocene
434 because of the absence of a significant change of the AMOC and the meltwater forcing

435 after 6 ka (Liu et al., 2014b). So we use the amplified anomalies between the cold and
436 warm periods, rather than simply the cold anomalies against the long-term average, to
437 illustrate the mechanisms of the event. We need to keep in mind that we still might not
438 be modeling the events comparable to the 4.2 ka BP event, particularly during the late
439 Holocene. More model-data, inter-model and inter-events comparisons are required to
440 better understand the cold events during the Holocene.

441

442

443 **Acknowledgments**

444 We acknowledge Prof. Bin Wang and two anonymous referees for the
445 comments helping to clarify and improve the paper. This research was jointly
446 supported by the National Key Research and Development Program of China (grant
447 no. 2016YFA0600401), the National Basic Research Program (grant no.
448 2015CB953804), the National Natural Science Foundation of China (grant nos.
449 41671197, 41420104002 and 41631175), Open Funds of State Key Laboratory of
450 Loess and Quaternary Geology, Institute of Earth Environment, CAS
451 (SKLLQG1820), and the Priority Academic Development Program of Jiangsu Higher
452 Education Institutions (PAPD, grant no. 164320H116). TraCE-21ka was made
453 possible by the DOE INCITE computing program, and supported by NCAR, the
454 NSFP2C2 program, and the DOE Abrupt Change and EaSM programs.
455

456 **References:**

- 457 Alley, R., and Agustsdottir, A.: The 8k event: cause and consequences of a major Holocene abrupt
458 climate change, *Quaternary Science Reviews*, 24, 1123-1149, 10.1016/j.quascirev.2004.12.004,
459 2005.
- 460 An, C.-B., Tang, L., Barton, L., and Chen, F.-H.: Climate change and cultural response around 4000
461 cal yr B.P. in the western part of Chinese Loess Plateau, *Quaternary Research*, 63, 347-352,
462 10.1016/j.yqres.2005.02.004, 2005.
- 463 Bond, G., Kromer, B., Beer, J., Muscheler, R., Evans, M. N., Showers, W., Hoffmann, S., Lotti-
464 Bond, R., Hajdas, I., and Bonani, G.: Persistent solar influence on North Atlantic climate during
465 the Holocene, *Science*, 294, 2130, 2001.
- 466 Booth, R. K., Jackson, S. T., Forman, S. L., Kutzbach, J. E., Bettis, I. E. A., Kreig, J., and Wright,
467 D. K.: A severe centennial-scale drought in mid-continental North America 4200 years ago and
468 apparent global linkages, *The Holocene*, 15, 321-328, 2005.
- 469 Bretherton, C. S., Widmann, M., Dymnikov, V. P., Wallace, J. M., and Bladé, I.: The effective
470 number of spatial degrees of freedom of a time-varying field, *J. Climate*, 12(7), 1990-2009,
471 1999.
- 472 Broccoli, A. J., Dahl, K. A., and Stouffer, R. J.: Response of the ITCZ to Northern Hemisphere
473 cooling, *Geophysical Research Letters*, 33, L01702, 10.1029/2005gl024546, 2006.
- 474 Brown, N., and Galbraith, E. D.: Hosed vs. unhosed: interruptions of the Atlantic Meridional
475 Overturning Circulation in a global coupled model, with and without freshwater forcing,
476 *Climate of the Past*, 12, 1663-1679, 10.5194/cp-12-1663-2016, 2016.
- 477 Cai, Y., Zhang, H., Cheng, H., An, Z., Lawrence Edwards, R., Wang, X., Tan, L., Liang, F., Wang,
478 J., and Kelly, M.: The Holocene Indian monsoon variability over the southern Tibetan Plateau
479 and its teleconnections, *Earth and Planetary Science Letters*, 335-336, 135-144,
480 10.1016/j.epsl.2012.04.035, 2012.
- 481 Clark, P. U., Shakun, J. D., Baker, P. A., Bartlein, P. J., Brewer, S., Brook, E., Carlson, A. E., Cheng,
482 H., Kaufman, D. S., Liu, Z., Marchitto, T. M., Mix, A. C., Morrill, C., Otto-Bliesner, B. L.,
483 Pahnke, K., Russell, J. M., Whitlock, C., Adkins, J. F., Blois, J. L., Clark, J., Colman, S. M.,
484 Curry, W. B., Flower, B. P., He, F., Johnson, T. C., Lynch-Stieglitz, J., Markgraf, V., McManus,
485 J., Mitrovica, J. X., Moreno, P. I., and Williams, J. W.: Global climate evolution during the last
486 deglaciation, *Proceedings of the National Academy of Sciences of the United States of America*,
487 109, E1134-1142, 10.1073/pnas.1116619109, 2012.
- 488 Cullen, H. M., Kaplan, A., Arkin, P. A., and DeMenocal, P. B.: Impact of the North Atlantic
489 Oscillation on Middle Eastern climate and streamflow, *Climatic Change*, 55, 315-338, 2002.
- 490 Cullen, H., deMenocal, P., Hemming, S., Hemming, G., Brown, F. H., Guilderson, T., and Sirocko,
491 F.: Climate change and the collapse of the Akkadian empire: Evidence from the deep sea,
492 *Geology*, 28, 379-382, 2000.
- 493 Deininger, M., McDermott, F., Mudelsee, M., Werner, M., Frank, N., and Mangini, A.: Coherency
494 of late Holocene European speleothem $\delta^{18}O$ records linked to North Atlantic Ocean circulation,
495 *Climate Dynamics*, 49, 595-618, 10.1007/s00382-016-3360-8, 2017.
- 496 Delworth, T. L., and Zeng, F.: Multicentennial variability of the Atlantic meridional overturning
497 circulation and its climatic influence in a 4000 year simulation of the GFDL CM2.1 climate
498 model, *Geophysical Research Letters*, 39, L13702, 10.1029/2012gl052107, 2012.
- 499 Delworth, T. L., and Zeng, F.: The Impact of the North Atlantic Oscillation on Climate through Its

500 Influence on the Atlantic Meridional Overturning Circulation, *Journal of Climate*, 29, 941-962,
501 10.1175/jcli-d-15-0396.1, 2016.

502 Ding, Q., and Wang, B.: Circumglobal Teleconnection in the Northern Hemisphere summer, *Journal*
503 *of Climate*, 18, 3483-3505, 2005.

504 Finkenbinder, M. S., Abbott, M. B., and Steinman, B. A.: Holocene climate change in
505 Newfoundland reconstructed using oxygen isotope analysis of lake sediment cores, *Global and*
506 *Planetary Change*, 143, 251-261, 10.1016/j.gloplacha.2016.06.014, 2016.

507 Fisher, D., Osterberg, E., Dyke, A., Dahl-Jensen, D., Demuth, M., Zdanowicz, C., Bourgeois, J.,
508 Koerner, R. M., Mayewski, P., Wake, C., Kreutz, K., Steig, E., Zheng, J., Yalcin, K., Goto-
509 Azuma, K., Luckman, B., and Rupper, S.: The Mt Logan Holocene—late Wisconsinan isotope
510 record: tropical Pacific—Yukon connections, *The Holocene*, 18, 667-677,
511 10.1177/0959683608092236, 2008.

512 Fleitmann, D., Burns, S. J., Mangini, A., Mudelsee, M., Kramers, J., Villa, I., Neff, U., Al-Subbary,
513 A. A., Buettner, A., Hippler, D., and Matter, A.: Holocene ITCZ and Indian monsoon dynamics
514 recorded in stalagmites from Oman and Yemen (Socotra), *Quaternary Science Reviews*, 26,
515 170-188, 10.1016/j.quascirev.2006.04.012, 2007.

516 Forman, S., Oglesby, R., Markgraf, V., and Stafford, T.: Paleoclimatic significance of Late
517 Quaternary eolian deposition on the Piedmont and High Plains, Central United States, *Global*
518 *and Planetary Change*, 11, 35-55, 1995.

519 He, F., Shakun, J. D., Clark, P. U., Carlson, A. E., Liu, Z., Otto-Bliesner, B. L., and Kutzbach, J. E.:
520 Northern Hemisphere forcing of Southern Hemisphere climate during the last deglaciation,
521 *Nature*, 494, 81-85, 10.1038/nature11822, 2013.

522 He, F.: Simulating Transient Climate Evolution of the Last deglaciation with CCSM3, Doctor of
523 Philosophy, Atmospheric and Oceanic Sciences, University of Wisconsin-Madison, 161 pp.,
524 2011.

525 Huang, C. C., Pang, J., Zha, X., Su, H., and Jia, Y.: Extraordinary floods related to the climatic event
526 at 4200 a BP on the Qishuihe River, middle reaches of the Yellow River, China, *Quaternary*
527 *Science Reviews*, 30, 460-468, 10.1016/j.quascirev.2010.12.007, 2011.

528 Jansen, E., Overpeck, J. T., Briffa, K. R., Duplessy, J.-C., Joos, F., Masson-Delmotte, V., Olago, D.,
529 Otto-Bliesner, B., Peltier, W. R., Rahmstorf, S., Ramesh, R., Raynaud, D., Rind, D. H.,
530 Solomina, O., Villalba, R., and Zhang, D.: Palaeoclimate. In: *Climate Change 2007: The*
531 *Physical Science Basis*. , Cambridge University Press, Cambridge, United Kingdom and New
532 York, NY, USA, 2007.

533 Kim, J.-H., Rimbu, N., Lorenz, S. J., Lohmann, G., Nam, S.-I., Schouten, S., Rühlemann, C., and
534 Schneider, R. R.: North Pacific and North Atlantic sea-surface temperature variability during
535 the Holocene, *Quaternary Science Reviews*, 23, 2141-2154, 10.1016/j.quascirev.2004.08.010,
536 2004.

537 Klus, A., Prange, M., Varma, V., Tremblay, L. B., and Schulz, M.: Abrupt cold events in the North
538 Atlantic in a transient Holocene simulation, *Climate of the Past Discussions*, 1-23, 10.5194/cp-
539 2017-106, 2017.

540 Kushnir, Y., and Stein, M.: North Atlantic influence on 19th–20th century rainfall in the Dead Sea
541 watershed, teleconnections with the Sahel, and implication for Holocene climate fluctuations,
542 *Quaternary Science Reviews*, 29, 3843-3860, 10.1016/j.quascirev.2010.09.004, 2010.

543 Lauritzen, S.-E.: Reconstruction of Holocene climate records from speleothems, in: *Global Change*

544 in the Holocene, edited by: Mackay, A., Battarbee, R., Birks, H. J. B., and Oldfield, F., Arnold,
545 London, 242-263, 2003.

546 Li, J., Sun, C., and Jin, F.-F.: NAO implicated as a predictor of Northern Hemisphere mean
547 temperature multidecadal variability, *Geophysical Research Letters*, 40, 5497-5502,
548 10.1002/2013gl057877, 2013.

549 Lin, J.-S., Wu, B., and Zhou, T.-J.: Is the interdecadal circumglobal teleconnection pattern excited
550 by the Atlantic multidecadal Oscillation?, *Atmospheric and Oceanic Science Letters*, 9, 451-
551 457, 10.1080/16742834.2016.1233800, 2016.

552 Liu, J. Q., Lv, H. Y., Negendank, J. F. W., Mingram, J., Luo, X. J., Wang, W. Y., and Chu, G. Q:
553 Cyclic of the Holocene climate variability in Huguangyan Maar lake, China, *Chinese Science*
554 *Bulletin (in Chinese)*, 45, 1190-1195, 2000.

555 Liu, Y. H., Sun, X., and Guo, C. Q.: Records of 4.2 ka BP Holocene Event from China and Its Impact
556 on Ancient Civilizations, *Geological Science and Technology Information (in Chinese)*, 32, 99-
557 106, 2013.

558 Liu, Z. Y., Otto-Bliesner, B., He, F., Brady, E. C., Tomas, R. A., Clark, P. U., Carlson, A. E., Lynch-
559 Stieglitz, J., Curry, W., Brook, E., Erickson, D. J., Jacob, R., Kutzbach, J., and Cheng, J.:
560 Transient simulation of Last Deglaciation with a new mechanism for Bolling-Allerod Warming,
561 *Science*, 325, 310-314, 2009.

562 Liu, Z., Carlson, A. E., He, F., Brady, E. C., Otto-Bliesner, B. L., Briegleb, B. P., Wehrenberg, M.,
563 Clark, P. U., Wu, S., Cheng, J., Zhang, J., Noone, D., and Zhu, J.: Younger Dryas cooling and
564 the Greenland climate response to CO₂, *Proceedings of the National Academy of Sciences of*
565 *the United States of America*, 109, 11101-11104, 10.1073/pnas.1202183109, 2012.

566 Liu, Z., Lu, Z., Wen, X., Otto-Bliesner, B. L., Timmermann, A., and Cobb, K. M.: Evolution and
567 forcing mechanisms of El Niño over the past 21,000 years, *Nature*, 515, 550-553,
568 10.1038/nature13963, 2014a.

569 Liu, Z., Zhu, J., Rosenthal, Y., Zhang, X., Otto-Bliesner, B. L., Timmermann, A., Smith, R. S.,
570 Lohmann, G., Zheng, W., and Elison Timm, O.: The Holocene temperature conundrum,
571 *Proceedings of the National Academy of Sciences of the United States of America*, 111, E3501-
572 3505, 10.1073/pnas.1407229111, 2014b.

573 Ljung, K., Björck, S., Renssen, H., and Hammarlund, D.: South Atlantic island record reveals a
574 South Atlantic response to the 8.2 kyr event, *Clim. Past*, 4, 35-45, 2008.

575 Ma, Z. X., Huang, J. H., Wei, Y., Li, J. H., and Hu, C. Y.: Organic carbon isotope records of the
576 Poyang Lake sediments and their implications for the paleoclimate during the last 8 ka,
577 *Geochimica (in Chinese)*, 33, 279-285, 10.19700/j.0379-1726.2004.03.007, 2004.

578 Marchant, R., and Hooghiemstra, H.: Rapid environmental change in African and South American
579 tropics around 4000 years before present: a review, *Earth-Science Reviews*, 66, 217-260,
580 10.1016/j.earscirev.2004.01.003, 2004.

581 Matero, I. S. O., Gregoire, L. J., Ivanovic, R. F., Tindall, J. C., and Haywood, A. M.: The 8.2 ka
582 cooling event caused by Laurentide ice saddle collapse, *Earth and Planetary Science Letters*,
583 473, 205-214, 10.1016/j.epsl.2017.06.011, 2017.

584 Mayewski, P. A., Rohling, E. E., Curt Stager, J., Karlén, W., Maasch, K. A., Meeker, L. D., Meyerson,
585 E. A., Gasse, F., van Kereveld, S., Holmgren, K., Lee-Thorp, J., Rosqvist, G., Rack, F.,
586 Staubwasser, M., Schneider, R. R., and Steig, E. J.: Holocene Climate Variability, *Quaternary*
587 *Research*, 62, 243-255, 10.1016/j.yqres.2004.07.001, 2004.

588 Morrill, C., LeGrande, A. N., Renssen, H., Bakker, P., and Otto-Bliesner, B. L.: Model sensitivity
589 to North Atlantic freshwater forcing at 8.2 ka, *Climate of the Past*, 9, 955-968, 10.5194/cp-9-
590 955-2013, 2013.

591 Morrill, C., Ward, E. M., Wagner, A. J., Otto-Bliesner, B. L., and Rosenbloom, N.: Large sensitivity
592 to freshwater forcing location in 8.2 ka simulations, *Paleoceanography*, 29, 930-945,
593 10.1002/2014pa002669, 2014.

594 Nakamura, A., Yokoyama, Y., Maemoku, H., Yagi, H., Okamura, M., Matsuoka, H., Miyake, N.,
595 Osada, T., Adhikari, D. P., Dangol, V., Ikehara, M., Miyairi, Y., and Matsuzaki, H.: Weak
596 monsoon event at 4.2 ka recorded in sediment from Lake Rara, Himalayas, *Quaternary*
597 *International*, 397, 349-359, 10.1016/j.quaint.2015.05.053, 2016.

598 Ning, L., Liu, J., Bradley, R. S., and Yan, M.: Comparing the spatial patterns of climate change in
599 the 9th and 5th millennia BP from TRACE-21 model simulations, *Climate of the Past*, 15, 41-
600 52, 10.5194/cp-15-41-2019, 2019.

601 Owen, L. A., and Dortch, J. M.: Nature and timing of Quaternary glaciation in the Himalayan–
602 Tibetan orogen, *Quaternary Science Reviews*, 88, 14-54, 10.1016/j.quascirev.2013.11.016,
603 2014.

604 Peltier, W. R.: GLOBAL GLACIAL ISOSTASY AND THE SURFACE OF THE ICE-AGE EARTH:
605 The ICE-5G (VM2) Model and GRACE, *Annual Review of Earth and Planetary Sciences*, 32,
606 111-149, 10.1146/annurev.earth.32.082503.144359, 2004.

607 Peng, Y., Xiao, J., Nakamura, T., Liu, B., and Inouchi, Y.: Holocene East Asian monsoonal
608 precipitation pattern revealed by grain-size distribution of core sediments of Daihai Lake in
609 Inner Mongolia of north-central China, *Earth and Planetary Science Letters*, 233, 467-479,
610 10.1016/j.epsl.2005.02.022, 2005.

611 Ramos-Román, M. J., Jiménez-Moreno, G., Camuera, J., García-Alix, A., Anderson, R. S., Jiménez-
612 Espejo, F. J., and Carrión, J. S.: Holocene climate aridification trend and human impact
613 interrupted by millennial- and centennial-scale climate fluctuations from a new sedimentary
614 record from Padul (Sierra Nevada, southern Iberian Peninsula), *Climate of the Past*, 14, 117-
615 137, 10.5194/cp-14-117-2018, 2018.

616 Rimbu, N., Lohmann, G., Lorenz, S. J., Kim, J. H., and Schneider, R. R.: Holocene climate
617 variability as derived from alkenone sea surface temperature and coupled ocean-atmosphere
618 model experiments, *Climate Dynamics*, 23, 215-227, 10.1007/s00382-004-0435-8, 2004.

619 Roland, T. P., Caseldine, C. J., Charman, D. J., Turney, C. S. M., and Amesbury, M. J.: Was there a
620 ‘4.2 ka event’ in Great Britain and Ireland? Evidence from the peatland record, *Quaternary*
621 *Science Reviews*, 83, 11-27, 10.1016/j.quascirev.2013.10.024, 2014.

622 Rupper, S., Roe, G., and Gillespie, A.: Spatial patterns of Holocene glacier advance and retreat in
623 Central Asia, *Quaternary Research*, 72, 337-346, 10.1016/j.yqres.2009.03.007, 2009.

624 Sachs, J. P.: Cooling of Northwest Atlantic slope waters during the Holocene, *Geophysical Research*
625 *Letters*, 34, L03609, 10.1029/2006gl028495, 2007.

626 Shakun, J. D., Clark, P. U., He, F., Marcott, S. A., Mix, A. C., Liu, Z., Otto-Bliesner, B., Schmittner,
627 A., and Bard, E.: Global warming preceded by increasing carbon dioxide concentrations during
628 the last deglaciation, *Nature*, 484, 49-54, 10.1038/nature10915, 2012.

629 Shanahan, T. M., Overpeck, J. T., Anchukaitis, K. J., Beck, J. W., Cole, J. E., Dettman, D. L., Peck,
630 J. A., Scholz, C. A., and King, J. W.: Atlantic forcing of persistent drought in West Africa,
631 *Science*, 324, 377-380, 2009.

632 Sigl, M., Severi, M., and McConnell, J. R.: A role for volcanoes in causing the "4.2 ka BP event"?,
633 The 4.2 ka BP event: an international workshop, Pisa, Italy, 2018.

634 Solomina, O. N., Bradley, R. S., Hodgson, D. A., Ivy-Ochs, S., Jomelli, V., Mackintosh, A. N., Nesje,
635 A., Owen, L. A., Wanner, H., Wiles, G. C., and Young, N. E.: Holocene glacier fluctuations,
636 Quaternary Science Reviews, 111, 9-34, 10.1016/j.quascirev.2014.11.018, 2015.

637 Staubwasser, M., and Weiss, H.: Holocene Climate and Cultural Evolution in Late Prehistoric–Early
638 Historic West Asia, Quaternary Research, 66, 372-387, 10.1016/j.yqres.2006.09.001, 2006.

639 Staubwasser, M., Sirocko, F., Grootes, P. M., and Segl, M.: Climate change at the 4.2 ka BP
640 termination of the Indus valley civilization and Holocene south Asian monsoon variability,
641 Geophysical Research Letters, 30, No. 8, 1425, 10.1029/2002gl016822, 2003.

642 Tan, L. C., An, Z. S., Cai, Y. J., and Long, H.: The Hydrological Exhibition of 4.2 ka BP Event in
643 China and Its Global Linkages, Geological Review (in Chinese), 54, 94-104,
644 10.16509/j.georeview.2008.01.010, 2008.

645 Tan, L. C., Cai, Y. J., Cheng, H., Edwards, L. R., Gao, Y. L., Xu, H., Zhang, H. W., and An, Z. S.:
646 Centennial- to decadal- scale monsoon precipitation variations in the upper Hanjiang River
647 region, China over the past 6650 years, Earth and Planetary Science Letters, 482, 580-590,
648 10.1016/j.epsl.2017.11.044, 2018.

649 Thompson, L. G., Mosley-Thompson, E., Davis, M., Henderson, K. A., Brecher, H., Zagorodnov,
650 V. S., Mashiotta, T., Lin, P. N., Mikhaleenko, V. N., Hardy, D. R., and Beer, J.: Kilimanjara Ice
651 Core Records: Evidence of Holocene Climate Change in Tropical Africa, Science, 298, 589-
652 593, 10.1126/science.1073198, 2002.

653 Tremblay, L. B., Mysak, L. A., and Dyke, A. S.: Evidence from driftwood records for century-to-
654 millennial scale variations of the high latitude atmospheric circulation during the Holocene,
655 Geophysical Research Letters, 24, 2027-2030, 10.1029/97gl02028, 1997.

656 Turney, C., Baillie, M., Clemens, S., Brown, D., Palmer, J., Pilcher, J., Reimer, P., and Leuschner,
657 H. H.: Testing solar forcing of pervasive Holocene climate cycles, Journal of Quaternary
658 Science, 20, 511-518, 10.1002/jqs.927, 2005.

659 Vellinga, M., and Wood, R. A.: Global climatic impacts of a collapse of the Atlantic Thermohaline
660 Circulation, Climatic Change, 54, 251-267, 2002.

661 Wagner, A. J., Morrill, C., Otto-Bliesner, B. L., Rosenbloom, N., and Watkins, K. R.: Model support
662 for forcing of the 8.2 ka event by meltwater from the Hudson Bay ice dome, Climate Dynamics,
663 41, 2855-2873, 10.1007/s00382-013-1706-z, 2013.

664 Walker, M. J. C., Berkelhammer, M., Björck, S., Cwynar, L. C., Fisher, D. A., Long, A. J., Lowe, J.
665 J., Newnham, R. M., Rasmussen, S. O., and Weiss, H.: Formal subdivision of the Holocene
666 Series/Epoch: a Discussion Paper by a Working Group of INTIMATE (Integration of ice-core,
667 marine and terrestrial records) and the Subcommission on Quaternary Stratigraphy
668 (International Commission on Stratigraphy), Journal of Quaternary Science, 27, 649-659,
669 10.1002/jqs.2565, 2012.

670 Wang, S. W.: 4.2ka BP Event, Advances in Climate Change Research (in Chinese), 6, 75-76, 2010.

671 Wang, S. W.: Holocene cold events in the North Atlantic: Chronology and Climate Impact,
672 Quaternary Sciences (in Chinese), 29, 1146-1153, 2009.

673 Wang, Y. J., Cheng, H., Edwards, L. R., He, Y. Q., Kong, X. G., An, Z. S., Wu, J. Y., Kelly, M.,
674 Dykoski, C. A., and Li, X. D.: The Holocene Asian Monsoon: Links to Solar Changes and
675 North Atlantic Climate, Science, 308, 854-857, 2005.

676 Wanner, H., Beer, J., Bütikofer, J., Crowley, T. J., Cubasch, U., Flückiger, J., Goosse, H., Grosjean,
677 M., Joos, F., Kaplan, J. O., Küttel, M., Müller, S. A., Prentice, I. C., Solomina, O., Stocker, T.
678 F., Tarasov, P., Wagner, M., and Widmann, M.: Mid- to Late Holocene climate change: an
679 overview, *Quaternary Science Reviews*, 27, 1791-1828, 10.1016/j.quascirev.2008.06.013,
680 2008.

681 Weiss, H., and Bradley, R. S.: What drives societal collapse?, *Science*, 291, 609-610, 2001.

682 Weiss, H., Courty, M. A., Wetterstrom, W., Guichard, F., Senior, L., Meadow, R., and Curnow, A.:
683 The Genesis and Collapse of Third Millennium North Mesopotamian Civilization, *Science*,
684 261, 995-1004, 10.1126/science.261.5124.995, 1993.

685 Weiss, H.: Global megadrought, societal collapse and resilience at 4.2-3.9 ka BP across the
686 Mediterranean and west Asia, *Past Global Change Magazine*, 24, 62-63,
687 10.22498/pages.24.2.62, 2016.

688 Weiss, H.: Megadrought, Collapse, and Resilience in late 3rd millennium BC Mesopotamia, 7th
689 Archaeological Conference of Central Germany, Halle (Saale), 2015.

690 Wu, W. X., and Liu T. S.: 4000aB.P. Event and its implications for the origin of Ancient Chinese
691 Civilization, *Quaternary Sciences (in Chinese)*, 21, 443-451, 2001.

692 Wu, W. X., and Liu, T. S.: Possible role of the “Holocene Event 3” on the collapse of Neolithic
693 Cultures around the Central Plain of China, *Quaternary International*, 117, 153-166,
694 10.1016/s1040-6182(03)00125-3, 2004.

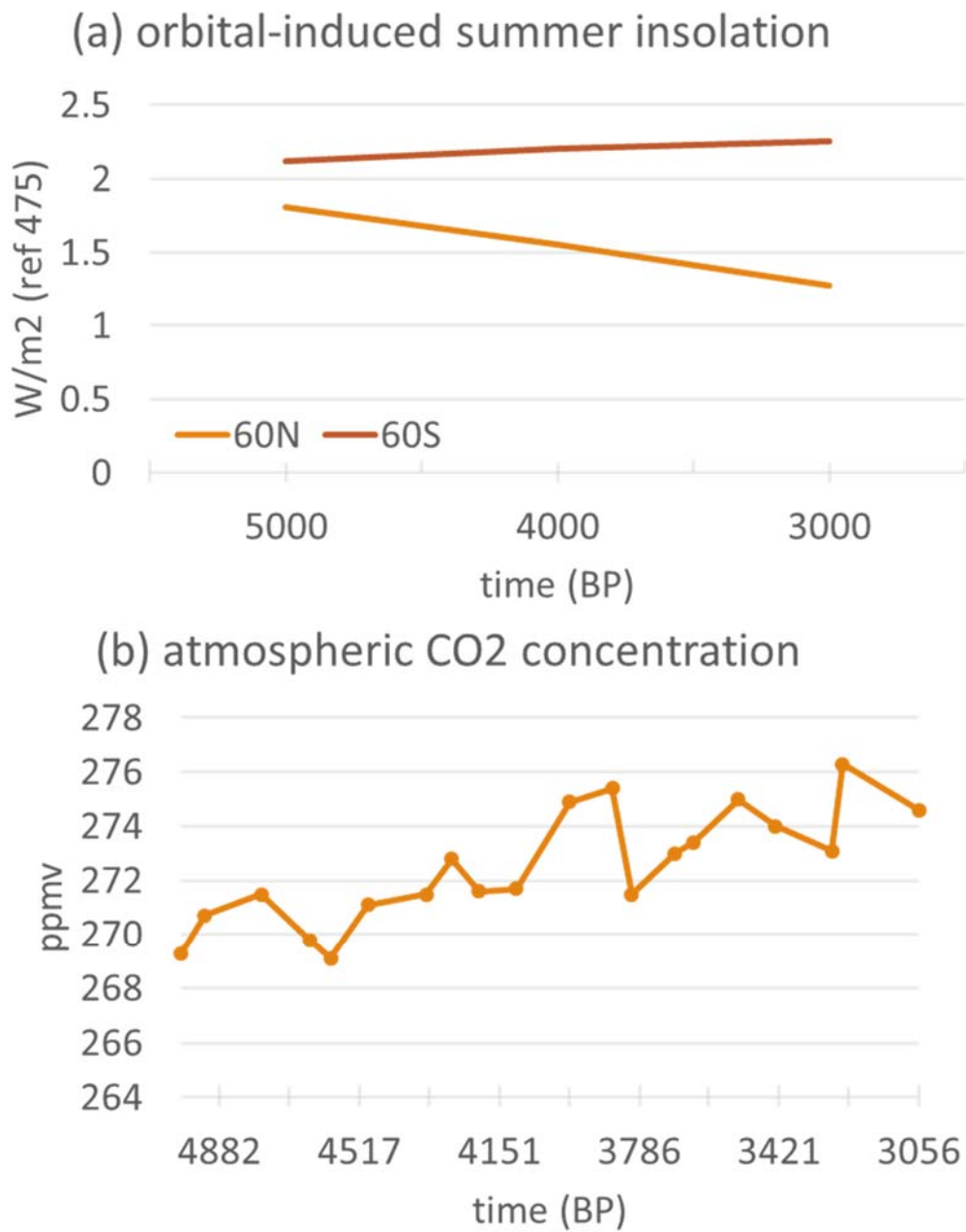
695 Yang, X. P., Scuder, L. A., Wang, X. L., Scuder, L. J., Zhang, D. G., Li, H. W., and al, e.:
696 Groundwater sapping as the cause of irreversible desertification of Hunshandake Sandy Lands,
697 Inner Mongolia, northern China, *PNAS*, 112, 702-706, 2015.

698 Yechieli, Y., Magaritz, M., Levy, Y., Weber, U., Kafri, U., Woelfli, W., and Bonani, G.: Late
699 Quaternary Geological History of the Dead Sea Area, Israel, *Quaternary Research*, 39, 59-67,
700 10.1006/qres.1993.1007, 1993.

701 Zhang, R., and Delworth, T. L.: Simulated Tropical Response to a Substantial Weakening of the
702 Atlantic Thermohaline Circulation, *Journal of Climate*, 18, 1853-1860, 2005.

703 Zhang, R., and Delworth, T. L.: Impact of Atlantic multidecadal oscillations on India/Sahel rainfall
704 and Atlantic hurricanes, *Geophysical Research Letters*, 33, L17712, 10.1029/2006gl026267,
705 2006.

706



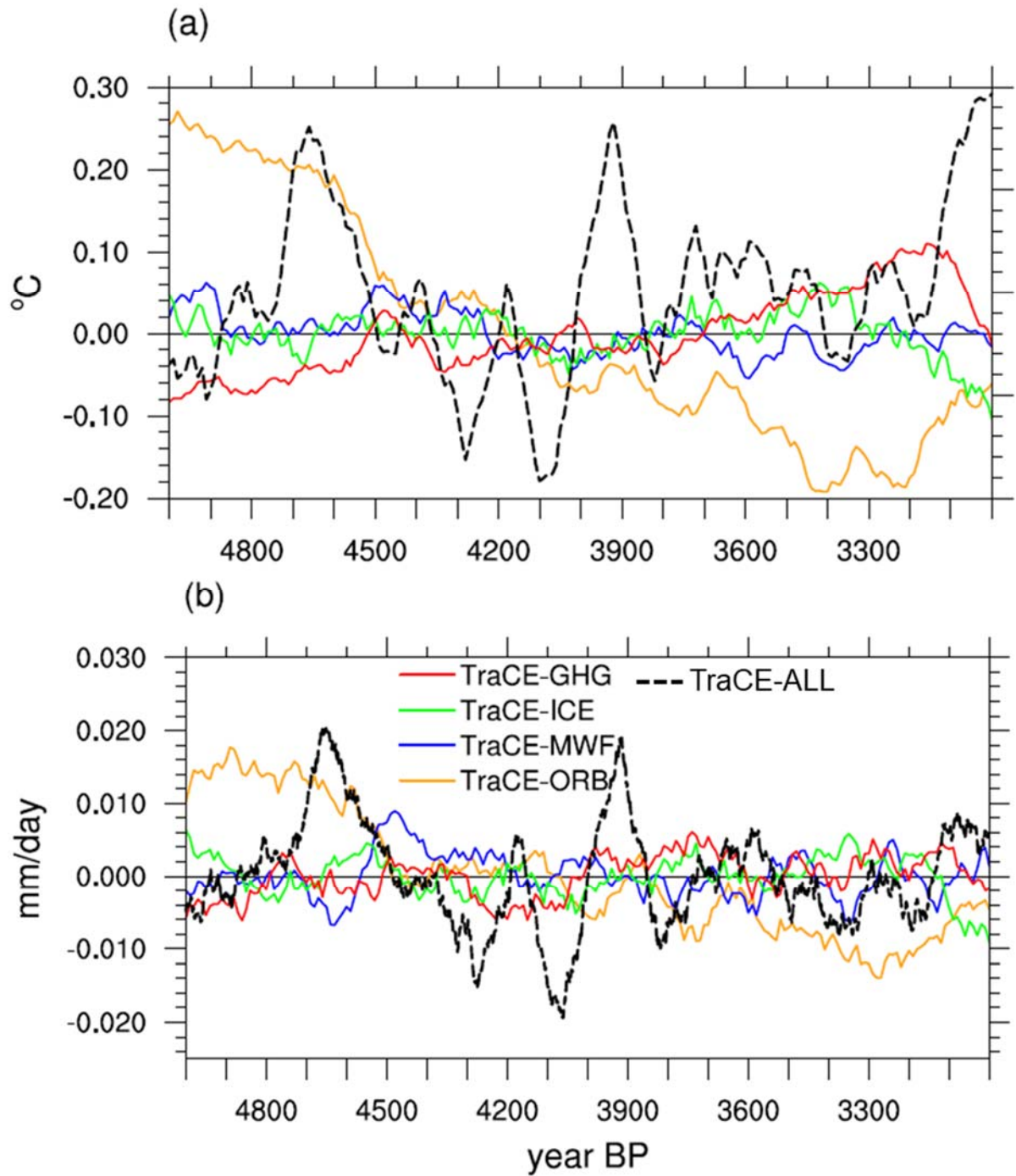
708

709 **Figure 1** Time series of (a) transient summer insolation (at 60°N and 60°S) changes710 resulted from the orbital variation and (b) the transient CO₂ change used in the

711 simulations.

712

713



715

716 **Figure 2** Time series of annual mean NH (a) surface temperature anomalies and (b)

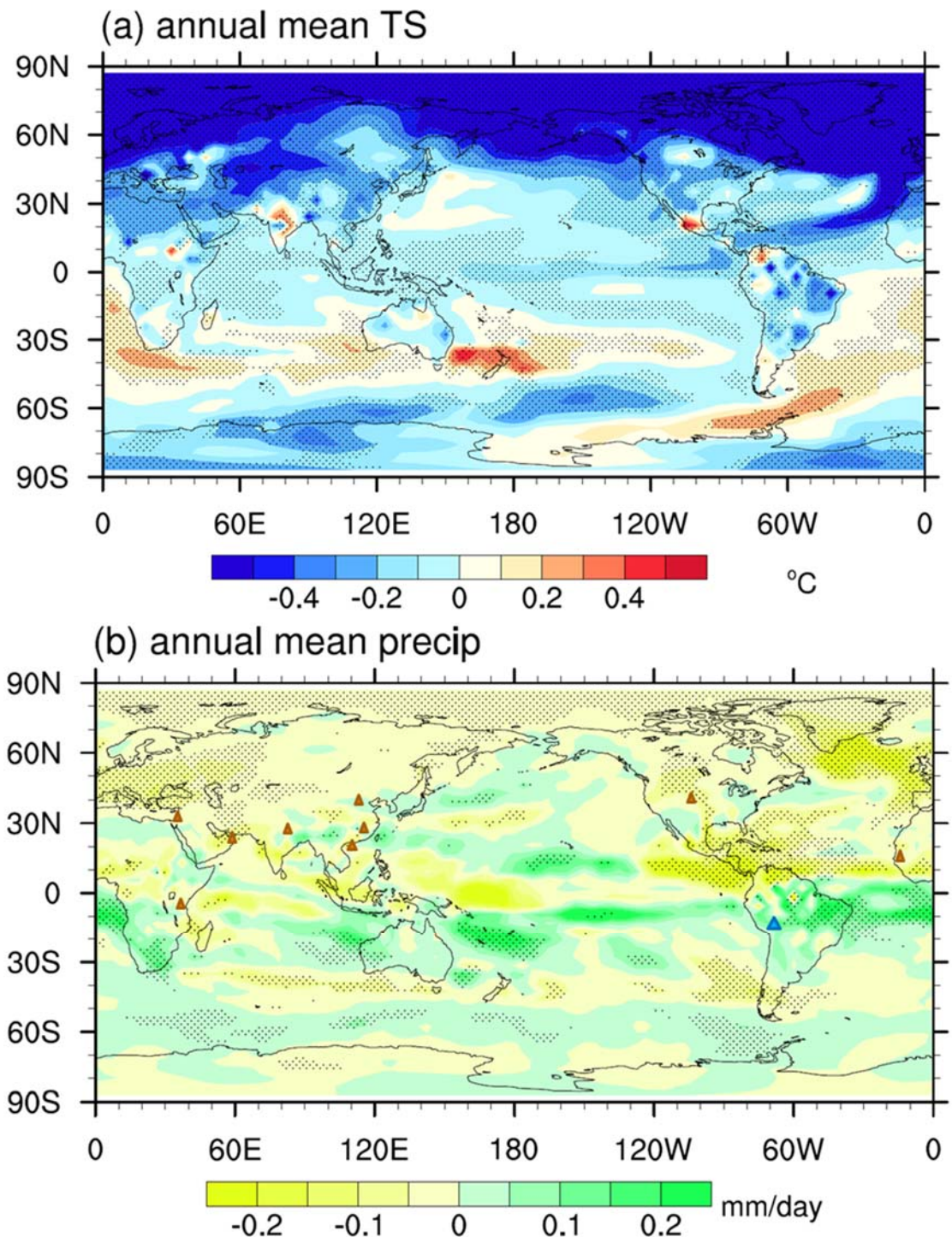
717 precipitation anomalies derived from the TraCE-ALL run (dashed black lines) and

718 each single forcing runs (solid color lines) from 5 ka BP to 3 ka BP. A 101-year

719 running mean has been applied to the time series.

720

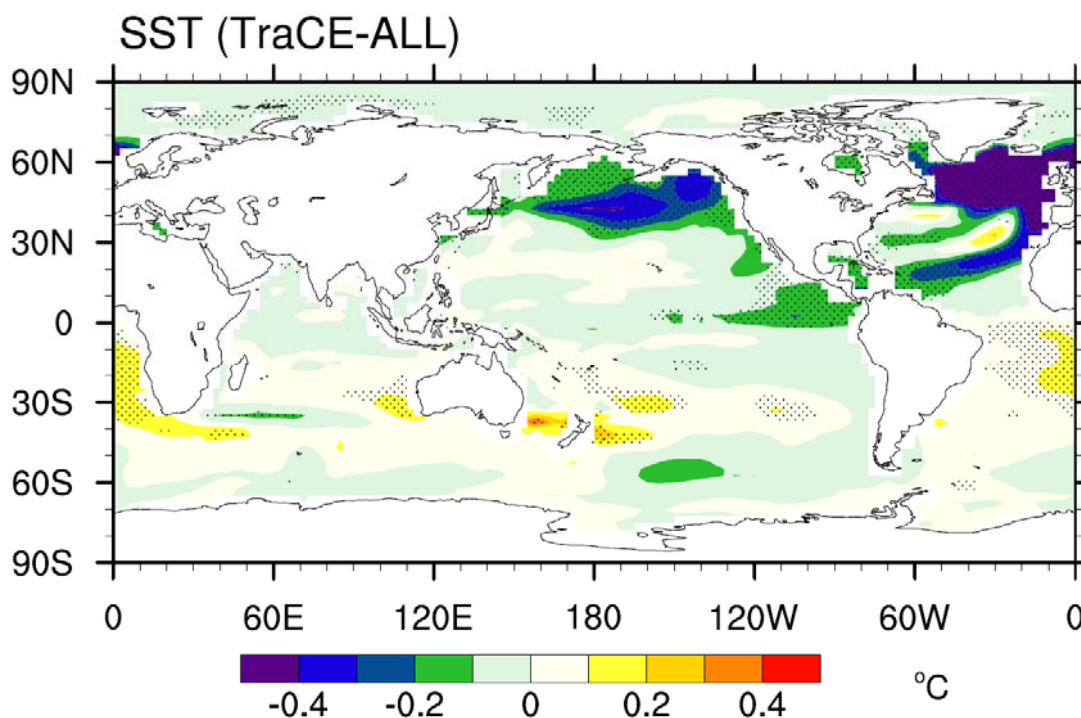
721
722
723



724
725 **Figure 3** Spatial distribution of the annual mean (a) surface temperature and (b)
726 precipitation differences between the cold periods and warm periods derived from the
727 TraCE-ALL run. Those regions where significant above 95% confidence level are
728 dotted. Triangles in (b) denote the dry (orange) and wet (blue) conditions documented

729 in the records, including the following sites: Kilimanjaro ($3^{\circ}04.6'S$, $37^{\circ}21.2'E$)
730 (Thompson et al., 2002), Dead Sea (Yechieli et al., 1993), Gulf of Oman ($24^{\circ}23.4'N$,
731 $59^{\circ}2.5'E$) (Cullen et al., 2000), Lake Rara ($29^{\circ}32'N$, $82^{\circ}05'E$) (Nakamura et al.,
732 2016), Maar lake in Huguangyan ($21.15^{\circ}N$, $110.29^{\circ}E$) (Liu et al., 2000), Daihai Lake
733 ($40.58^{\circ}N$, $112.7^{\circ}E$) (Peng et al., 2005), Poyang Lake ($29.15^{\circ}N$, $116.27^{\circ}E$) (Ma et al.,
734 2004), Eastern Colorado Dunes ($40^{\circ}20'N$, $104^{\circ}16'E$) (Forman et al., 1995), Lake
735 Titicaca ($12.08^{\circ}S$, $69.85^{\circ}W$) and Lake Guiers ($16.3^{\circ}N$, $16.5^{\circ}W$) (Marchant and
736 Hooghiemstra, 2004).

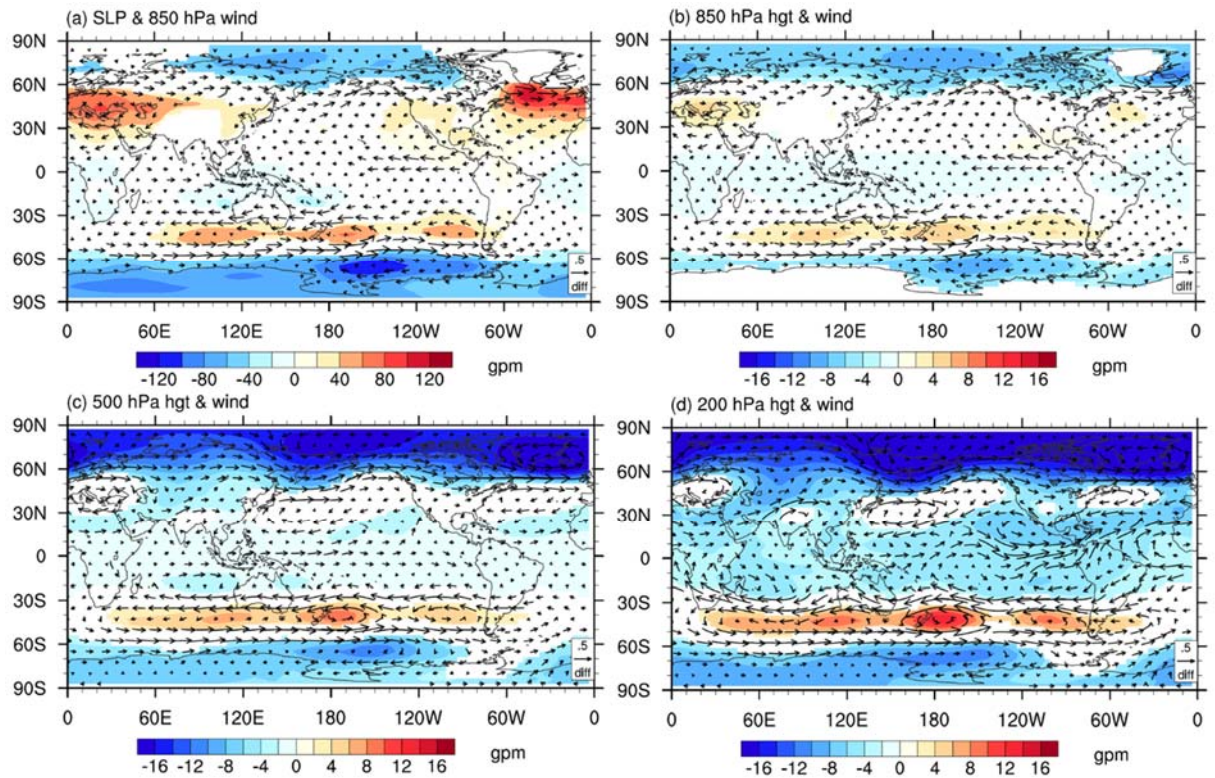
737
738
739
740
741



742
743 **Figure 4** Spatial distribution of annual mean SST difference between the cold and
744 warm periods derived from the TraCE-ALL run. Those regions where significant
745 above 95% confidence level are dotted.
746
747

748

749



750

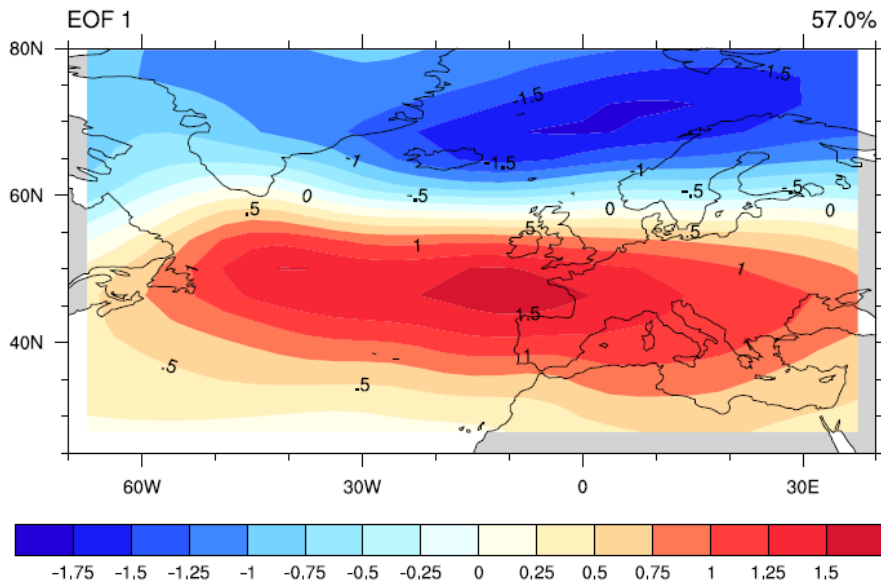
751 **Figure 5** Differences of annual mean (a) sea level pressure and 850 hPa wind, (b)
752 geopotential height and wind on 850 hPa, (c) geopotential height and wind on 500
753 hPa and (d) geopotential height and wind on 200 hPa between cold and warm periods
754 derived from the TraCE-ALL run. Those regions where significant above 95%
755 confidence level are plotted.

756

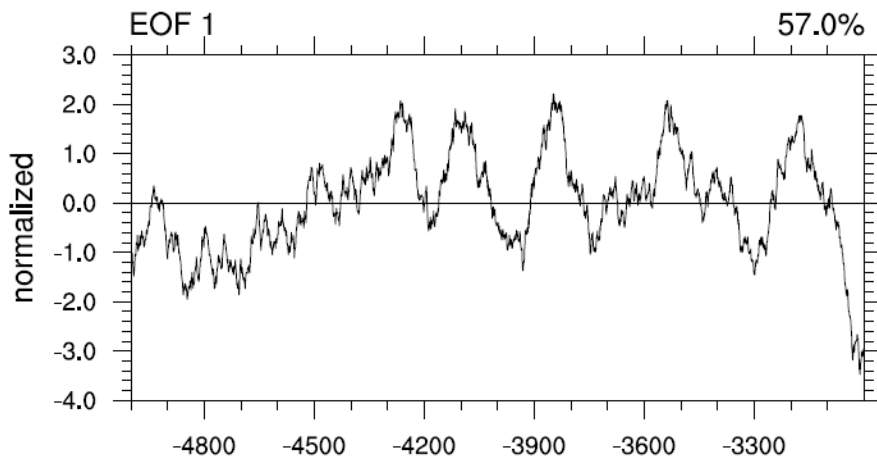
757

758

759
760



761

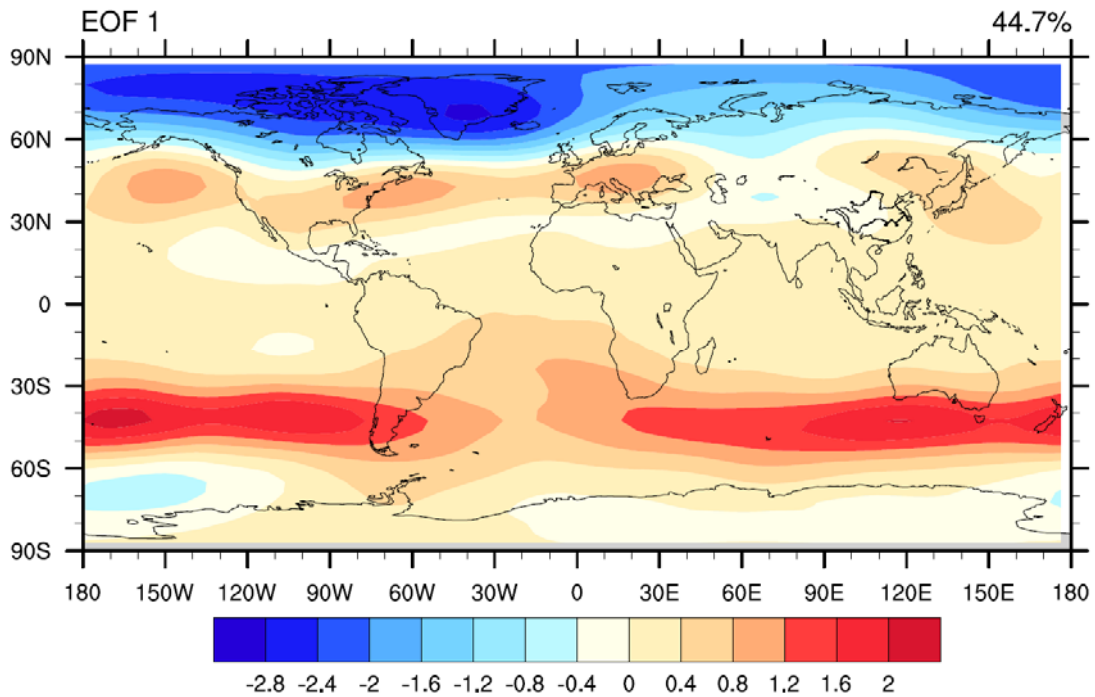


762

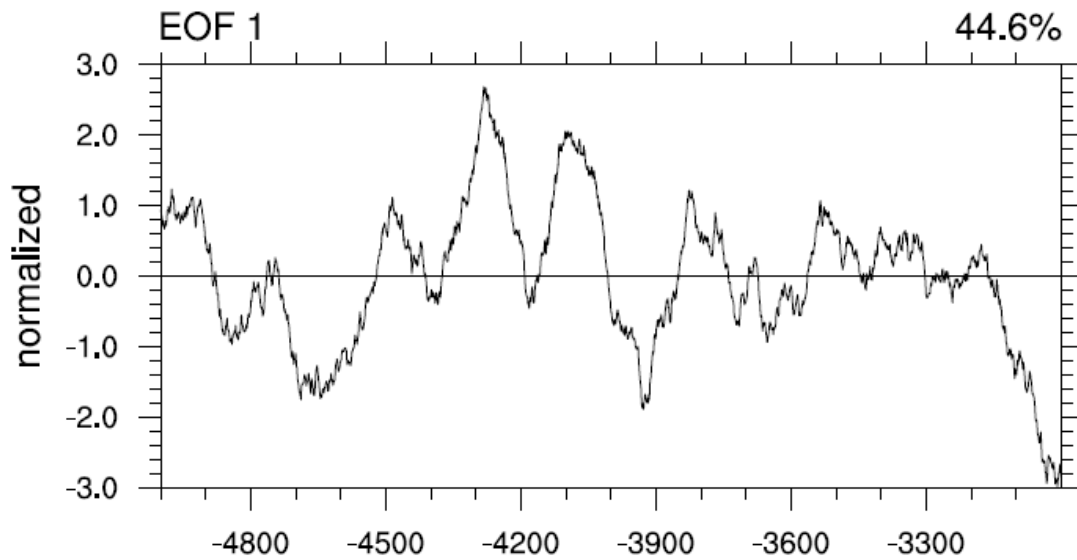
763 **Figure 6** Standardized first leading mode of the EOF of annual mean SLP over the
764 North Atlantic region (70W-40E, 25N-80N) during the period of 5.0 ka BP to 3.0 ka
765 BP derived from the TraCE-ALL run, after application of a 101-year running mean.
766 The spatial distribution is shown in the top panel, and the time series is shown in the
767 bottom panel. Only this mode passed the North test for EOF.

768
769
770
771
772

773
774
775



776

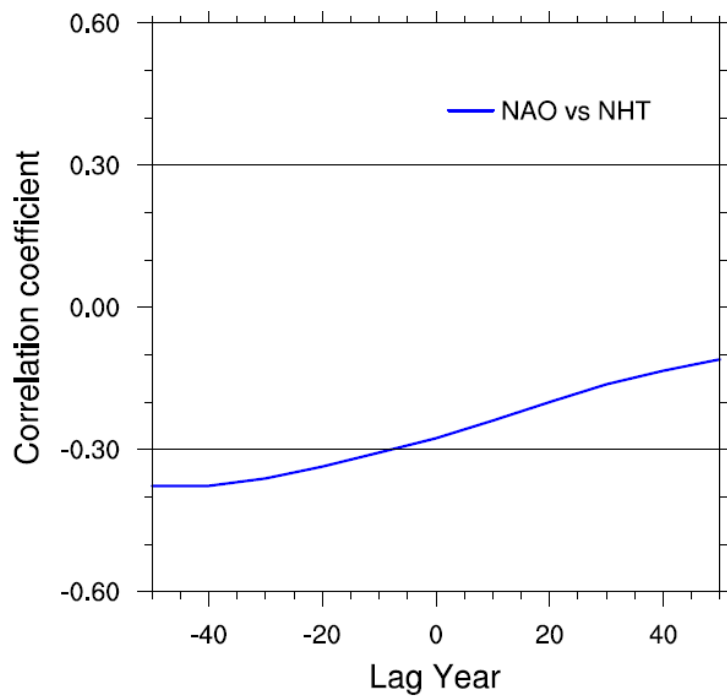


777

778 **Figure 7** Standardized first leading mode of the EOF of annual mean geopotential
779 height at 200 hPa during the period of 5.0 ka BP to 3.0 ka BP derived from the TraCE-
780 ALL run, after application of a 101-year running mean. The spatial distribution is
781 shown in the top panel, and the time series is shown in the bottom panel. Only this
782 mode passed the North test for EOF.

783

784



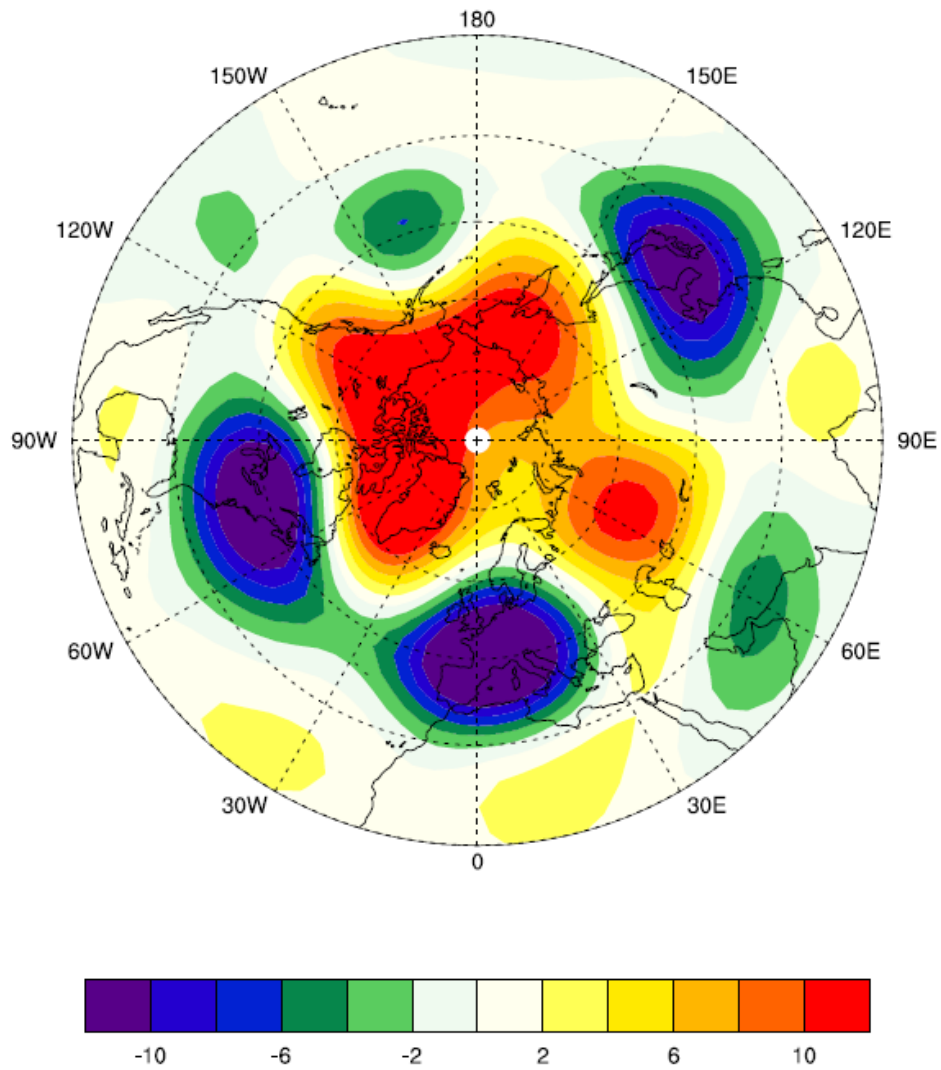
785

786 **Figure 8** Lead-lag correlation between the annual mean North Atlantic Oscillation
787 (NAO) and the North Hemisphere Surface Temperature (NHT) during 4.4 ka BP-4.0
788 ka BP derived from the TraCE-ALL run. The black lines (± 0.3) show the significance
789 levels ($p < 0.05$).

790

791

792



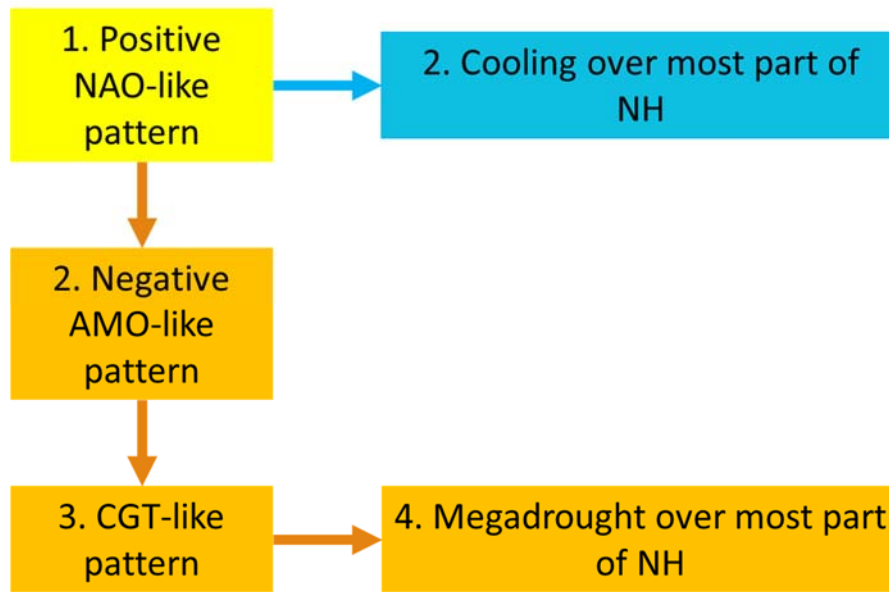
793

794 **Figure 9** Annual mean geopotential height regressed against the SST over the North
 795 Atlantic during 5.0 ka BP - 3.0 ka BP derived from the TraCE-ALL run, after 31-year
 796 running mean application.

797

798

799



800

801 **Figure 10** Schematic diagram shown the mechanisms behind the 4.2 ka BP event.

802

803

804

805 **Table 1** The information of the experiments used in this study.

Experiments	Forcings	Time spanning	Temporal resolution
TraCE-ALL	Orbital, melt-water flux, continental ice-sheet, and Greenhouse gases	22000 BP to 1990 CE	Monthly mean
TraCE-ORB	Orbital only	22000 BP to 1990 CE	Decadal mean
TraCE-MWF	Melt-water flux only	19000 BP to 1990 CE	Decadal mean
TraCE-ICE	Continental ice-sheets only	19000 BP to 1990 CE	Decadal mean
TraCE-GHG	Greenhouse gases only	22000 BP to 1990 CE	Decadal mean

806

807

808

809

810

811

812 **Table 2** Correlation coefficients between the annual mean and seasonal mean NHTs

813 derived from the TraCE-ALL run and those from each single-forcing run from 5.0 ka

814 BP to 3.0 ka BP.

Single forcing run	Annual mean	JJA mean	DJF mean
TraCE-ORB	-0.05	0.79	-0.12
TraCE-MWF	-0.18	0.48	-0.43
TraCE-ICE	-0.30	-0.20	-0.18
TraCE-GHG	0.14	-0.73	0.40

815

816